

JGR Space Physics

RESEARCH ARTICLE

10.1029/2020JA029078

Special Section:

Geospace multi-point observations in Van Allen Probes and Arase era

Key Points:

- We report unique simultaneous ground and magnetospheric satellite observations of two isolated proton auroras at subauroral latitudes
- Van Allen Probes observed two EMIC waves at ~ 1 and 0.4 Hz during crossings of the isolated proton auroras
- When the EMIC waves were observed, 5–20 keV proton flux was locally enhanced near a steep density decrease in the plasmopause region

Correspondence to:

K. Nakamura,
nakamura.koki@isee.nagoya-u.ac.jp

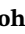
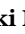

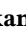

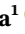


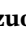



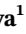
Citation:

Nakamura, K., Shiokawa, K., Otsuka, Y., Shinbori, A., Miyoshi, Y., Connors, M., et al. (2021). Simultaneous observation of two isolated proton auroras at subauroral latitudes by a highly sensitive all-sky camera and Van Allen Probes. *Journal of Geophysical Research: Space Physics*, 126, e2020JA029078. <https://doi.org/10.1029/2020JA029078>

Received 27 DEC 2020

Accepted 26 APR 2021

Simultaneous Observation of Two Isolated Proton Auroras at Subauroral Latitudes by a Highly Sensitive All-Sky Camera and Van Allen Probes

Kohki Nakamura¹ , Kazuo Shiokawa¹ , Yuichi Otsuka¹ , Atsuki Shinbori¹ , Yoshizumi Miyoshi¹ , Martin Connors² , Harlan Spence³ , Geoff Reeves⁴ , Herbert O. Funsten⁴ , Robert MacDowall⁵ , Charles Smith³ , John Wygant⁶ , and John Bonnell⁶ 

¹Institute for Space-Earth Environmental Research, Nagoya University, Nagoya, Japan, ²Athabasca University, Athabasca, AB, Canada, ³University of New Hampshire, Durham, NH, USA, ⁴Los Alamos National Laboratory, Los Alamos, NM, USA, ⁵NASA's Goddard Space Flight Center, Greenbelt, MD, USA, ⁶University of California, Berkeley, CA, USA

Abstract Isolated proton auroras (IPAs) appearing at subauroral latitudes are generated by energetic protons precipitating from the magnetosphere through interaction with electromagnetic ion cyclotron (EMIC) waves. An IPA thus indicates the spatial scale and temporal variation of wave-particle interactions in the magnetosphere. In this study, a unique event of simultaneous ground and magnetospheric satellite observations of two IPAs were conducted on March 16, 2015, using an all-sky imager at Athabasca, Canada and Van Allen Probes. The Van Allen Probes observed two isolated EMIC waves with frequencies of ~ 1 and 0.4 Hz at $L \approx 5.0$ when the satellite footprint crossed over the two IPAs. This suggests that the IPAs were caused by localized EMIC waves. Proton flux at 5–20 keV increased locally when the EMIC waves appeared. Electron flux at energies below ~ 500 eV also increased. Temperature anisotropy of the energetic protons was estimated at 1.5–2.5 over a wide L -value range of 3.0–5.2. Electron density gradually decreased from $L = 3.5$ to 5.4, suggesting that the EMIC wave at $L \approx 5.0$ was located in the gradual plasmopause. From these observations, we conclude that the localized IPAs and associated EMIC waves took place because of localized enhancement of energetic proton flux and plasma density structure near the plasmopause. The magnetic field observed by the satellite showed small variation during the wave observation, indicating that the IPAs were accompanied by the weak field-aligned current.

Plain Language Summary Isolated proton aurora (IPA) appearing at subauroral latitudes ($\sim 55^\circ$ – 65°) is generated by energetic protons precipitating from Earth's magnetosphere, possibly through interaction with plasma waves called electromagnetic ion cyclotron (EMIC) waves. The IPA indicates the spatial scale and temporal variation of wave-particle interactions in the magnetosphere. EMIC waves are expected to contribute to the rapid loss of radiation-belt particles into the atmosphere. Thus, IPAs present essential information related to EMIC waves. In this study, we report unique simultaneous ground and magnetospheric satellite observations of two IPAs using an all-sky imager at Athabasca, Canada and Van Allen Probes acquired on March 16, 2015. Van Allen Probes observed two isolated EMIC waves with frequencies of ~ 1 and 0.4 Hz when the satellite footprint crossed over the two IPAs. This indicates that the IPAs were caused by localized EMIC waves. We conclude that the localized IPAs and associated EMIC waves took place due to localized enhancement of energetic proton number flux and local plasma density structure near the plasmopause.

1. Introduction

Auroras at high-latitude ionosphere are caused by precipitation of electrons and ions from the magnetosphere, and thus, reveal dynamic plasma variation in the magnetosphere. The emission mechanism of proton auroras differs from that of electron auroras. Although electrons can move only along magnetic field lines, protons can move across magnetic field lines when they are neutralized to hydrogen through charge-exchange collisions (Vegard, 1939). Isolated proton auroras (IPAs) are one of the proton auroras which are observed simultaneously with Pc1 geomagnetic pulsations at subauroral latitudes. They have latitudinal widths of a few degrees and longitudinal widths of 250–800 km (e.g., Sakaguchi et al., 2008, 2016).

Electromagnetic ion cyclotron (EMIC) waves have been considered to be the cause of proton precipitation from the magnetosphere to generate IPAs. EMIC waves are plasma waves excited by ion cyclotron instability near the magnetic equatorial plane, and are considered to be one of the major causes of the loss of radiation-belt electrons and ring current ions (e.g., Albert, 2003; Miyoshi et al., 2008; Omura & Zhao, 2012, 2013; Summers & Thorne, 2003; Thorne et al., 2006). Note that other generation processes for EMIC waves, such as mode conversions (Miyoshi et al., 2019), have been investigated. EMIC waves interact with energetic protons in the magnetosphere through ion cyclotron resonance to scatter the proton pitch angle and cause their precipitation into the ionosphere. EMIC waves are generated by hot (typically 10–100 keV) anisotropic ions ($T_{\text{perp}} > T_{\text{par}}$, where T_{perp} and T_{par} are respectively ion temperatures perpendicular and parallel to the magnetic field lines) overlapping with cold dense plasma populations (Cornwall et al., 1970). EMIC waves occur more at higher L shells in the magnetosphere (e.g., Keika et al., 2013; Min et al., 2012). On the other hand, the plasmopause and plasmaspheric plumes have been suggested as favorable locations for EMIC wave occurrence enhancement (Fraser et al., 1989; Horne & Thorne, 1993; Morley et al., 2009; Pickett et al., 2010). Usanova et al. (2013) reported that EMIC waves were around 20 times more likely to be observed inside plasmaspheric plumes than outside.

In previous satellite observations, isolated proton precipitation at energies of 30–80 keV was observed by the POES satellites simultaneously with Pc1 geomagnetic pulsations observed by ground-based induction magnetometers (Miyoshi et al., 2008; Yahnina et al., 2000, 2002, 2003, 2007). Nishimura et al. (2014) reported evolution of nightside subauroral proton aurora caused by transient plasma sheet flows with EMIC waves using simultaneous observations by ground auroral imagers and THEMIS and NOAA/POES satellites. In addition, when these ground induction magnetometers observed Pc1/EMIC waves, IPAs were observed by ground-based all-sky imagers (e.g., Miyoshi et al., 2008; Nomura et al., 2012; Sakaguchi et al., 2007, 2008). According to these reports, on/off timings of IPA emissions always coincided with the appearance and disappearance of ground Pc1/EMIC waves. Sakaguchi et al. (2008) showed that the IPA occurrence region tends to shift to lower (higher) latitudes with increasing (decreasing) frequency of simultaneous Pc1/EMIC waves. These frequencies are related to the ambient magnetic field intensity in the wave generation region. Thus, the relationship between the Pc1/EMIC wave frequency and the IPA latitude indicates that the IPA is related to the EMIC wave source region on the magnetic equatorial plane. Sakaguchi et al. (2016) reported that as the K_p index increases, the IPA occurrence rate increases and the local time of IPA appearance shifts toward duskside.

Despite these extensive previous works, there are few simultaneous observations of plasma and electromagnetic fields in IPA source regions in the magnetospheric equatorial plane, except for the above Nishimura et al. (2014). The IPA is a direct ionospheric projection of the wave-particle interaction region at a specific L value in the magnetosphere (e.g., Sakaguchi et al., 2016). Thus, simultaneous observations provide important information regarding EMIC wave-particle interaction regions. In this study, we report the simultaneous observation of two IPAs with associated Pc1/EMIC waves and their source regions in the inner magnetosphere, using an all-sky monochromatic imager and an induction magnetometer on the ground and Van Allen Probes (Probe A), and clarify the characteristics of plasma and electromagnetic fields in the source region of IPAs in the magnetosphere.

2. Instrumentation

In this analysis, we used data from ground-based auroral and geomagnetic field observations and Van Allen Probes acquired over 6 years (2013–2018). Auroral and geomagnetic field data were taken from Athabasca, Canada (54.6°N, 246.36°E, geomagnetic latitude 61.1°N [$L = 4.3$]).

An all-sky imager (imager #7) of the Optical Mesosphere Thermosphere Imagers (Shiokawa et al., 1999) was used for aurora observations. The imager has a highly sensitive cooled CCD camera that can capture faint emission of less than 1 R. The imager has seven interference filters that transmit only the emissions of specific wavelengths. In the present analysis, we use emissions of 486.1 nm ($H\beta$) to confirm proton precipitation and 557.7 nm (OI), which is caused by secondary electrons from proton precipitation. The structure of the IPA is more clearly confirmed by the 557.7-nm images. The sampling interval of these auroral images

is 2 min. The 557.7- and 486.1-nm intensities were converted to absolute values in Rayleigh units by using imager sensitivity data and sky background images at a 572.5-nm wavelength.

To confirm that the observed auroras are IPAs caused by EMIC waves, we also use data from an induction magnetometer of the ISEE Magnetometer Network at Athabasca (Shiokawa et al., 2010). This induction magnetometer can observe geomagnetic pulsations at a range of Pc1 frequency (0.2–5 Hz) with a sampling rate of 64 Hz.

In this study, we used Van Allen Probes launched on 30 August 2012 as an inner magnetosphere observer. For analyses, we used equipment onboard the Van Allen Probes, namely, the Electric Field and Wave Suite (EFW) (Wygant et al., 2013) to measure electric fields, the Electric and Magnetic Field Instrument Suite and Integrated Science (EMFISIS) (Kletzing et al., 2013) to measure magnetic and electric fields, and the Helium Oxygen Proton Electron (HOPE) instrument (Funsten et al., 2013) of the Energetic Particle, Composition, and Thermal Plasma Suite (Spence et al., 2013) to measure helium, oxygen, protons, and electrons at an energy range of 1 eV–50 keV.

3. Event Selection

To perform simultaneous observations of IPAs on the ground and EMIC waves in the inner magnetosphere, we selected clear nights from the 6 years of 2013–2018. Sky conditions were determined using hourly all-sky images classified into four categories: “s” (clear sky with stars), “p” (few clouds and many stars), “m” (many clouds and a few stars), and “c” (overcast or rain). These sky conditions are stored in a database at <http://stdb2.stelab.nagoya-u.ac.jp/omti/obslst.html>. For this study, we selected dates and times categorized as “s” or “p.”

For simultaneous observations of IPA source regions in the magnetosphere, the footprint of the Van Allen Probes in the ionosphere must be in a region where the IPA is observed on the ground. Therefore, from among the clear-sky nights selected above, we selected dates and times when the satellite footprint passed over the field-of-view of the all-sky imager at Athabasca (49.56–59.76°N, 241.52–251.72°E). This footprint was traced to an altitude of 100 km from the satellite orbit using the International Geomagnetic Reference Field (IGRF)-12 model (Thébault et al., 2015). Then, Pc1/EMIC waves were identified using dynamic spectra of the *H*- and *D*-components of the magnetic field obtained by the induction magnetometer at Athabasca. We selected clear monochromatic emissions appearing at a specific frequency range of 0.2–5 Hz as Pc1/EMIC waves.

We next extracted events where IPAs occur simultaneously with Pc1/EMIC waves. The IPA was identified as spot-like auroral structures extending in the east-west direction equatorward of the auroral oval. Proton emissions were confirmed from all-sky images taken by using the 486.1-nm interference filter.

Next, we determined the imager attitude using star positions in the all-sky image, and converted the all-sky image to geographic coordinates. Emission heights of 557.7 and 486.1 nm were assumed at an altitude of 120 km. By plotting the position of Van Allen Probes on the converted images, we confirmed whether the satellite footprint passed over the IPA. The magnetic field model used to calculate the footprint is the Tsyganenko 01 (T01) model (Tsyganenko, 2002a, 2002b) if the event date is in geomagnetically quiet time ($Dst > -25$ nT), and the Tsyganenko 04 (T04) model (Tsyganenko & Sitnov, 2005) in geomagnetically disturbed time ($Dst < -25$ nT).

Using these procedures, we identified three events during which the Van Allen Probes footprint simultaneously passed near the IPA from the 6-year analysis of 2013–2018. However, two of these (on April 9, 2015, 0500 UT and February 17, 2017, 0530 UT) were events where the satellite footprint did not actually pass over the IPA. The only perfect simultaneous observation event was on March 16, 2015 (0532–0544 UT and 0546–0549 UT). The time of this simultaneous observation was the recovery phase of a substorm with maximum AE index of ~ 400 nT at around 0455 UT, before the start of a magnetic storm. This study reports this simultaneous observation event in detail.

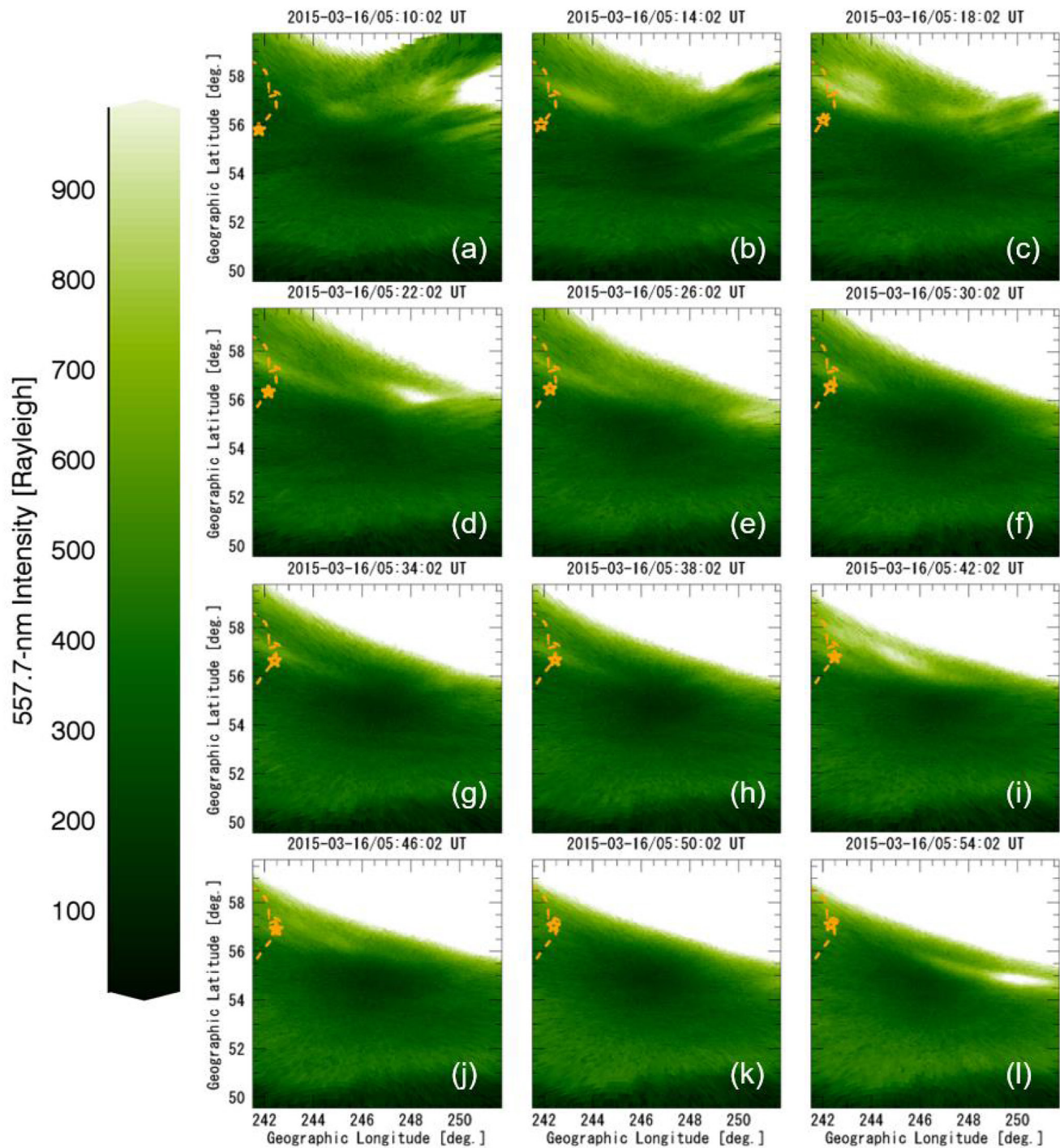


Figure 1. (a–l) Auroral images in geographical coordinates obtained on March 16, 2015 by an all-sky imager at Athabasca with a 557.7-nm interference filter. Yellow stars and dashed lines indicate the footprint of the Van Allen Probes (Probe A) orbit at an altitude of 120 km.

4. Results

4.1. Ground-Based Observation

Figures 1a–1l show auroral images in geographical coordinates obtained on March 16, 2015 by an all-sky imager at Athabasca with a 557.7-nm interference filter. The footprint of the Van Allen Probes (Probe A), mapped at an altitude of 120 km, is shown by the yellow star and dashed line. From the upper left to the

lower right, images every 4 min from 0510 to 0554 UT are shown. Since March 16, 2015 was a geomagnetically quiet period, we used the T01 model (Tsyganenko, 2002a, 2020b), which is optimized for such intervals, to estimate the footprint location. There is a persistent bright emission in the northeast of all 12 images, corresponding to the auroral oval. In Figures 1b–1j, several IPAs can be seen in the northwest at image centers as spot-like structures extending geomagnetically in the east-west direction a little South from the equatorward boundary of the auroral oval. The Van Allen Probes, indicated by the yellow star, passed over this aurora at 0532–0544 UT. At 0518, 0522, 0526, 0542, 0546, and 0554 UT, another IPA with similar structure and a stronger emission intensity appeared geomagnetically poleward of the previous IPA. The satellite footprint briefly touched this stronger IPA at 0546–0549 UT. After that, this poleward IPA disappeared when the Van Allen Probes footprint passed over this location at 0550–0554 UT.

Figures 2a–2l show auroral images in geographical coordinates obtained on March 16, 2015 by an all-sky imager at Athabasca with a 486.1-nm ($H\beta$) interference filter by the same method as those in Figure 1. The 486.1-nm emission is used to confirm proton precipitation. IPA structures similar to those in Figure 1 are clearly seen in the northwest of the images in Figures 2b–2j. A clear IPA emission appears at 0514, 0518, 0522, 0526, 0542, and 0554 UT, as in Figure 1. The emission in 486.1 nm is weak. However, the noise level of the CCD camera was estimated to be less than 2.4 R, and the observed auroral emission in 486.1 nm was much larger than this noise level. These images indicate that the observed spot-like IPAs extending geomagnetically in the east-west direction are caused by proton precipitation.

Figures 3a and 3b show temporal variations of 557.7- and 486.1-nm auroral images (shown in Figures 1 and 2) in north-south cross section (keogram), and Figure 3c shows H -component magnetic field spectra observed on March 16, 2015 by an induction magnetometer at Athabasca from 0400 to 0630 UT. The keograms in Figures 3a and 3b were obtained by converting 557.7- and 486.1-nm images in Figures 1 and 2 to altitude adjusted corrected geomagnetic (AACGM) coordinates (Shepherd, 2014) and averaging the auroral intensity for a longitudinal range of 303.63–312.30°E centered at the magnetic longitude of Athabasca (307.8°E) for each latitude. These rather wide integration longitudes are taken to monitor temporal variation of spot-like moving IPAs.

Figures 3a and 3b show that the time of the strong IPA emission appearing intermittently at a magnetic latitude of $\sim 64^\circ$ coincides with the appearance of Pc1 geomagnetic pulsations at a frequency of ~ 0.4 Hz. The pink arrow points to a weak IPA emission the Van Allen Probes passed over at 0532–0544 UT. Note that clear Pc1 geomagnetic pulsations were not observed in association with this IPA. The black arrow points to the time at 0546–0549 UT, when the satellite footprint briefly touched the stronger IPA emission at a higher latitude. A Pc1 wave with frequency ~ 0.4 Hz was observed at this time.

4.2. Van Allen Probes Observation

Figures 4a and 4b show the orbit of the Van Allen Probes (Probe A) in the magnetosphere in solar magnetic (SM) coordinates, with XY and XZ planes of the SM coordinates, respectively. The time when the Van Allen Probes passed over two IPAs (0532–0549 UT) is shown as the red segment in both. At the time of the simultaneous observation, the Van Allen Probes was at a radial distance of ~ 5 R_E near the magnetic equatorial plane in the premidnight sector.

Figures 5–8 show data obtained on March 16, 2015 by the Van Allen Probes (Probe A) from 0400 to 0630 UT. Magnetic local time (MLT), magnetic latitude (MLAT), and L values are shown at the bottom of each figure. The two pink dashed lines and two cyan dashed lines indicate time intervals when the Van Allen Probes footprint crossed over the IPAs at lower and higher latitudes, respectively.

Figures 5a and 5b, respectively, show proton and electron number fluxes observed by HOPE, and Figures 5c and 5d, respectively, show Y and Z components of the electric field spectra in modified geocentric solar ecliptic (MGSE) coordinates observed by EFW. In Figure 5a, plasma sheet ion flux can be continuously recognized after 0410 UT at energies above ~ 1 keV with increasing energies closer to the Earth (nose structure, Ejiri et al., 1980; Smith & Hoffman, 1974). Proton flux at an energy range of ~ 5 –20 keV increases rapidly around the time when the Van Allen Probes crossed over the two IPAs. In addition, electron flux at energies less than a few hundred electronvolts increases at these times. Figures 5c and 5d show a strong EMIC wave at a frequency of around 1 Hz, clearly corresponding to the time when the satellite crossed over the weaker

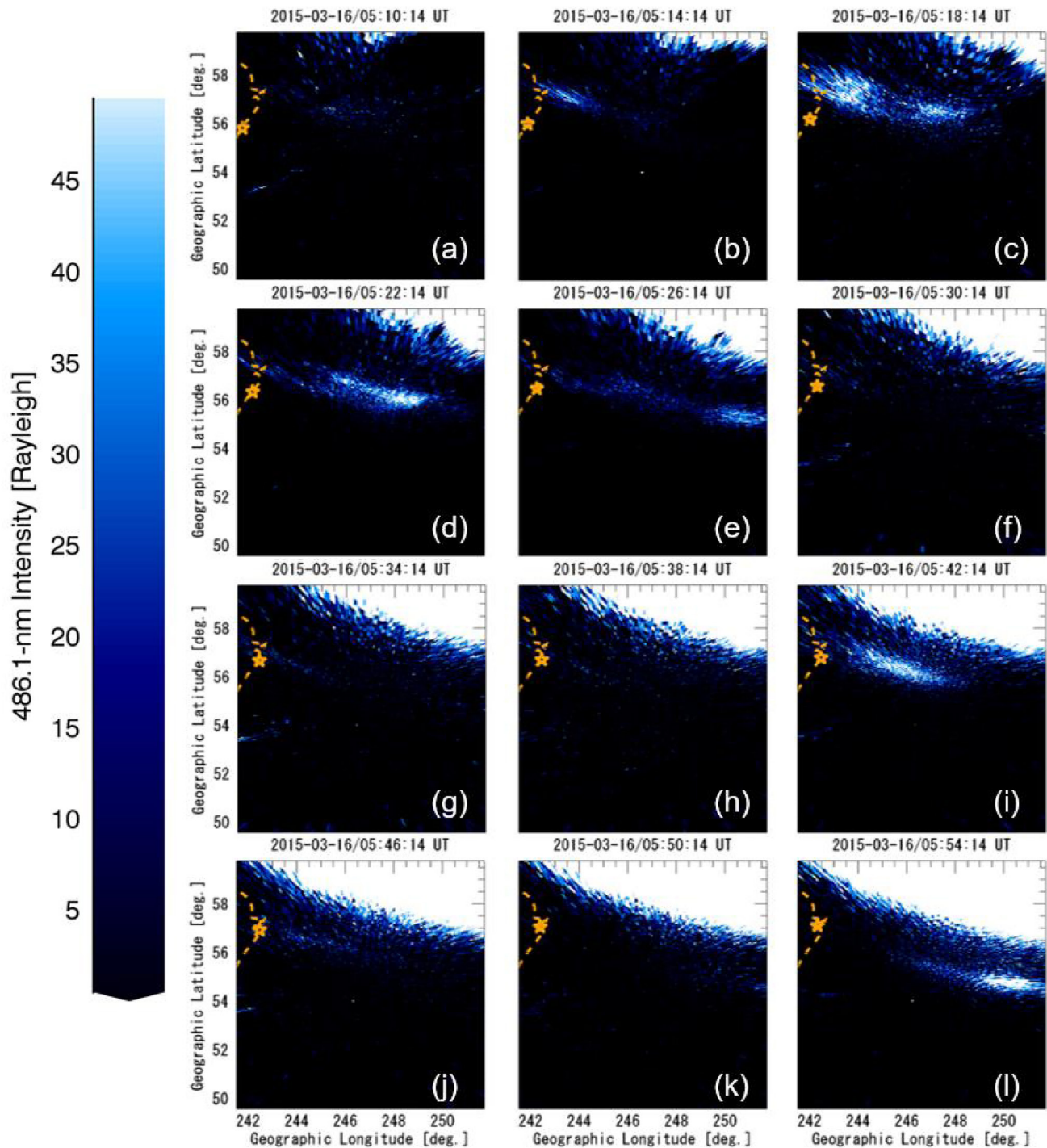


Figure 2. (a-l) Auroral images in geographical coordinates obtained on March 16, 2015 by an all-sky imager at Athabasca with a 486.1-nm interference filter. Yellow stars and dashed lines indicate the footprint of the Van Allen Probes (Probe A) orbit at an altitude of 120 km.

IPA at a lower latitude. This strongly suggests that the IPA observed on the ground was caused by the EMIC wave generated in the inner magnetosphere. There is a small timing delay of the start of the IPA crossings at 0532 UT (shown by the pink dashed line) from the EMIC waves at 0528 UT, which correspond to the latitudinal difference of $\sim 0.1^\circ$ in the footprint location in Figure 1. We will discuss possible causes of this discrepancy later in Section 5. The yellow lines in these panels show cyclotron frequencies of H^+ , He^+ , and O^+ . The frequency of this EMIC wave was between the H and He cyclotron frequencies.

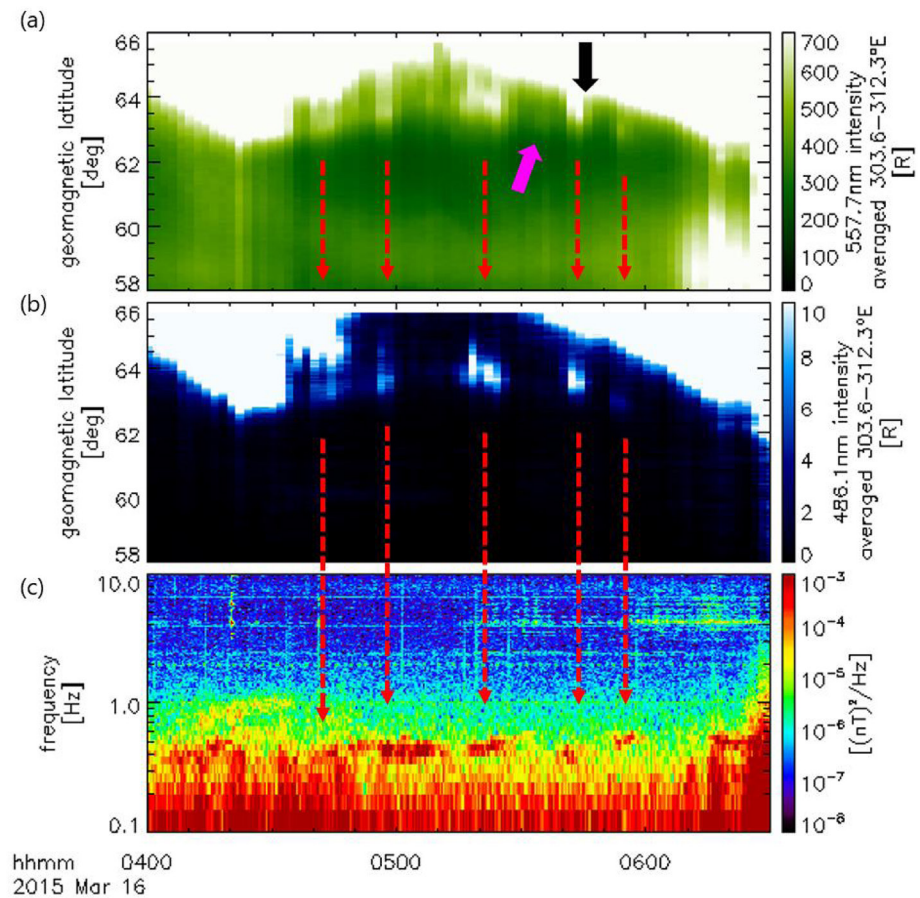


Figure 3. (a) Temporal variation of 557.7-nm and (b) 486.1-nm auroral images (shown in Figures 1 and 2) in north-south cross-sections (keograms) and (c) *H*-component magnetic field spectra observed on March 16, 2015 by an induction magnetometer at Athabasca from 0400 to 0630 UT. The red dotted lines indicate correspondence between the IPAs at magnetic latitude of $\sim 64^\circ$ and the Pc1 geomagnetic pulsations at ~ 0.4 Hz. The pink arrow points to the IPA emission the Van Allen Probes passed over at 0532–0544 UT. The black arrow points to the time at 0546–0549 UT when the satellite footprint briefly touched a stronger IPA emission at a higher latitude.

To investigate variations of electric and magnetic fields and plasma density associated with the IPA crossing, Figures 6a–6c show electric field variations in the MGSE coordinates observed by EFW, magnetic field variations observed by EMFISIS in SM coordinates while subtracting 10-min running averages, and the electron density estimated from the upper limit frequency of upper hybrid resonance waves observed by EMFISIS, respectively. Because the magnetic field weakens with satellite distance from the Earth, 10-min running averages were subtracted to eliminate effects of Earth's magnetic field.

In Figure 6a, characteristic electric field variations were not observed when the satellite footprint passed the two IPAs. Figure 6b shows rapid AC fluctuations with an amplitude of ± 3 nT especially in the B_y component, corresponding to the EMIC waves at a frequency range of ~ 1 and ~ 0.4 Hz, at the times of the IPA crossings. In addition, we observed the gradual decrease in B_y and increase in B_z with an amplitude of ~ 2 nT at 0532–0544 UT shown by the pink dashed lines in Figure 6. Electron density decreased from 0418 to 0600 UT and featured complexity and variability, indicating that the Van Allen Probes observed the EMIC waves in the plasmopause region. Note that electron density at the time of the IPA crossings was just before the sharp decrease of the density.

Figures 7a–7c show the *X*, *Y*, and *Z* components of the magnetic field spectra in SM coordinates, respectively. The yellow lines in these panels show the cyclotron frequencies of H^+ , He^+ , and O^+ . Similar to Figures 5c and 5d, an EMIC wave packet at a frequency range of ~ 1 Hz was clearly observed in these magnetic field spectra at the time of weaker IPA crossing at a lower latitude. Additionally, an EMIC wave at a frequency of

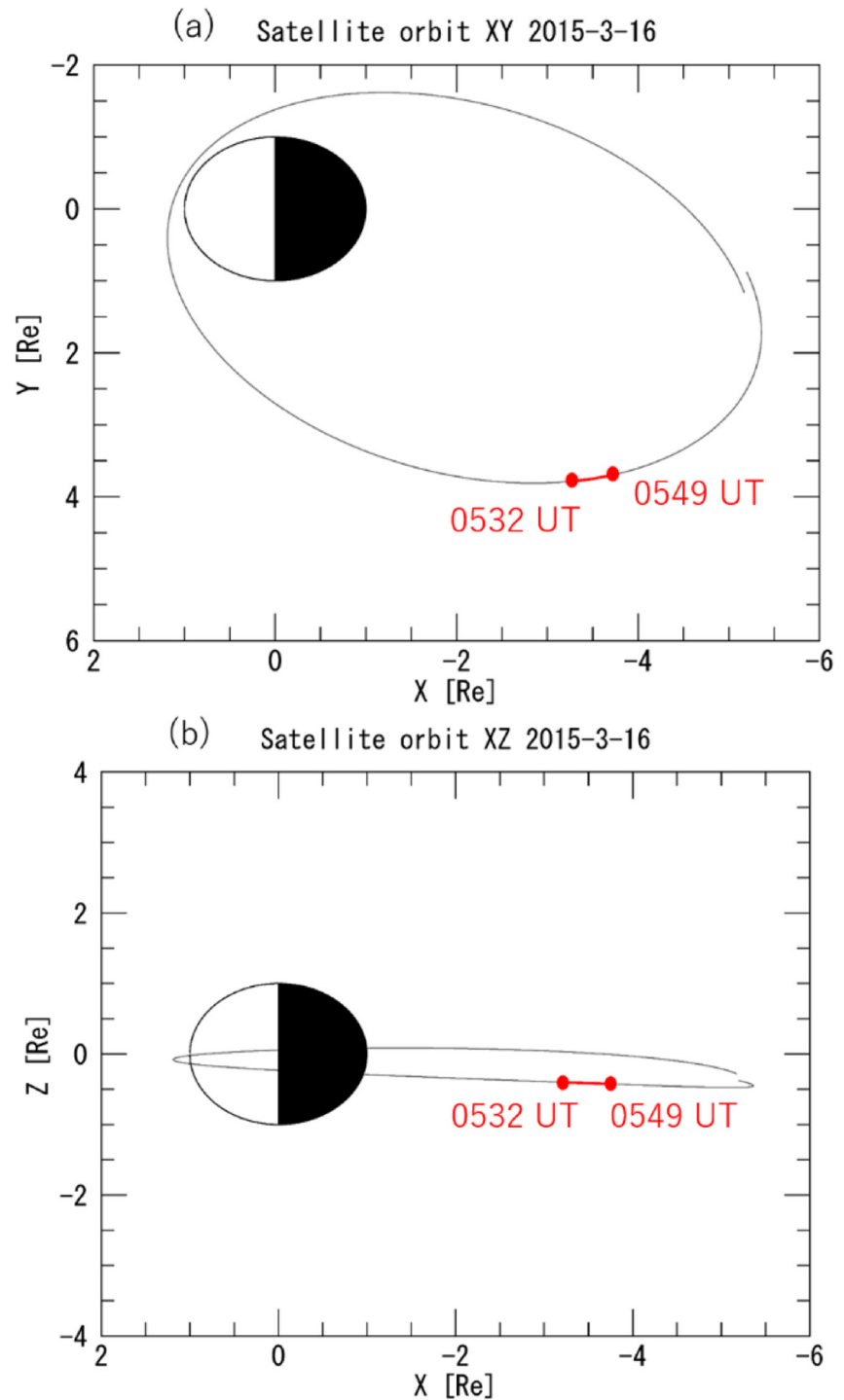


Figure 4. Orbit of the Van Allen Probes on (a) the XY plane and (b) the XZ plane in SM coordinates.

~0.4 Hz was observed at the time of the cyan dashed lines. This indicates a close relationship between the two EMIC waves and the two IPAs at lower and higher latitudes. The ~1- and 0.4-Hz waves are proton-band and helium-band EMIC waves, respectively, because the former appeared between H^+ and He^+ cyclotron frequencies and the latter appeared between He^+ and O^+ cyclotron frequencies. The ~0.4-Hz wave was not clearly identified in the electric field spectra in Figures 5c and 5d owing to artificial noise in this frequency range.

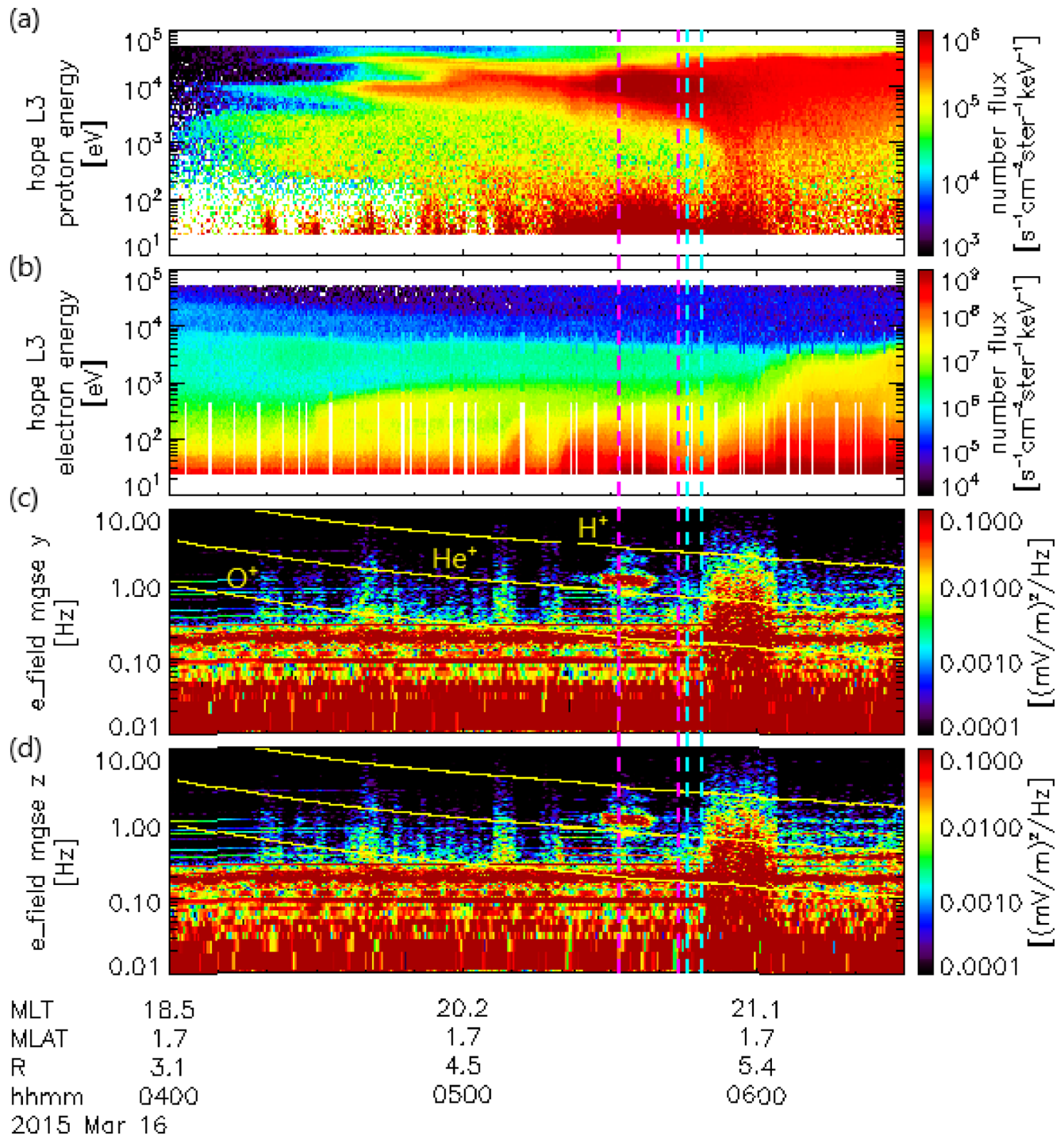


Figure 5. (a) Proton and (b) electron number fluxes observed by HOPE, and (c) Y and (d) Z components of electric field spectra in MGSE coordinates observed at 0400–0630 UT on March 16, 2015 by EFW onboard Van Allen Probes (Probe A). Pink and cyan dotted lines show time intervals when the Van Allen Probes footprint crossed over the two IPAs. Yellow lines show the cyclotron frequencies of H^+ , He^+ , and O^+ .

Figure 8 shows the proton temperatures and their anisotropy calculated from the distribution function of protons at energies of 1 eV–50 keV observed by HOPE. Figures 8a–8c respectively show proton temperature parallel to the magnetic field line (T_{par}) and perpendicular to the magnetic field line (T_{perp}), and proton temperature anisotropy (T_{perp} / T_{par}). T_{perp} was systematically larger than T_{par} , and T_{perp} / T_{par} was ~ 1.5 – 2.5 at 0400–0545 UT. This proton temperature anisotropy is favorable for generation of EMIC waves (Cornwall

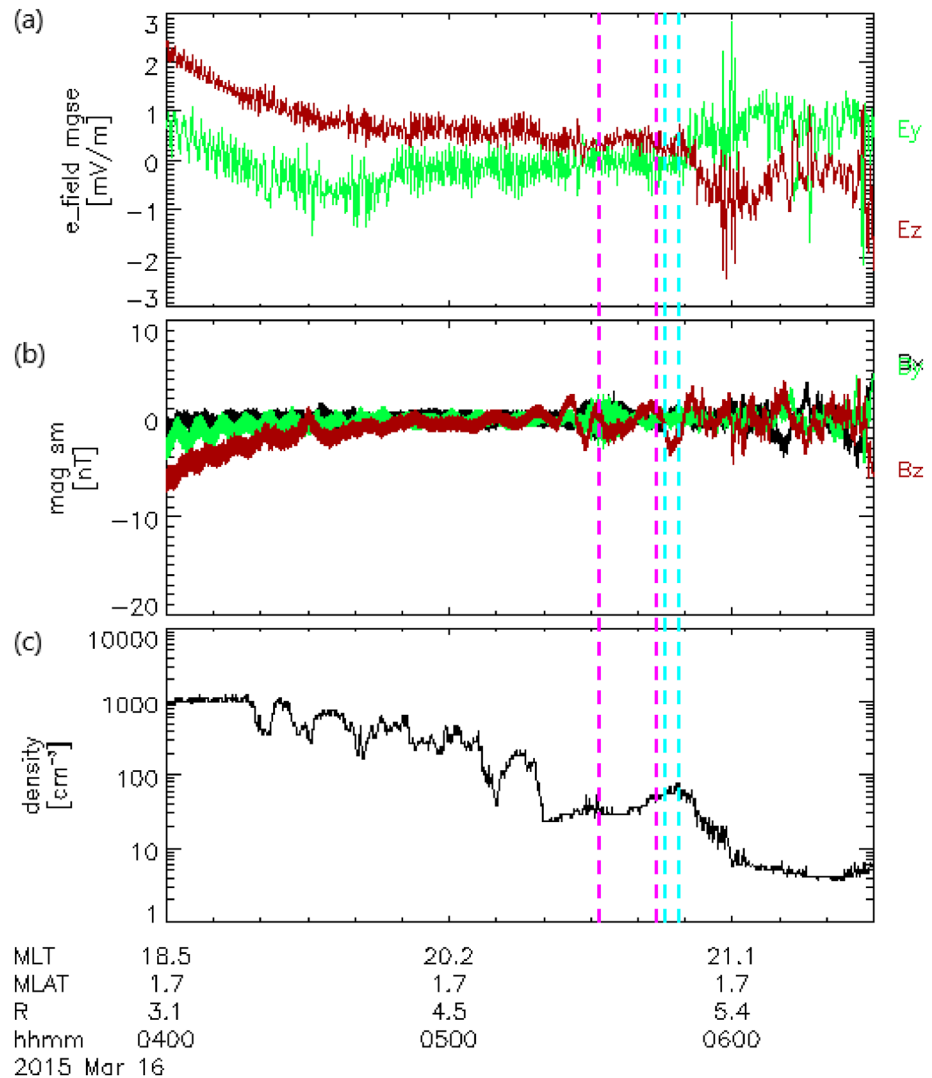


Figure 6. (a) Electric field variations in MGSE coordinates observed by EFW, (b) magnetic field variations observed by EMFISIS in SM coordinates, and (c) electron density observed at 0400–0630 UT on March 16, 2015 by EMFISIS from the upper hybrid resonance frequency. 10-min Running averages are subtracted from the original magnetic field variations in Figure 6b to eliminate effects of satellite motion in Earth’s magnetic field. Pink and cyan dotted lines show time intervals when the Van Allen Probes footprint crossed over the two IPAs.

et al., 1970). There is no particular enhancement of temperature anisotropy when the Van Allen Probes crossed the IPAs.

Figure 9 shows the proton flux anisotropy observed by HOPE, where (a–c) show proton number flux perpendicular and parallel to the magnetic field line and proton flux anisotropy, respectively. Anisotropy was estimated by calculating perpendicular flux divided by the parallel flux. For most of the plotted energy range, proton flux perpendicular to the magnetic field was larger than the parallel flux. There is no particular enhancement of temperature anisotropy at the time when the Van Allen Probes crossed the IPAs.

5. Discussion

The Van Allen Probes observed EMIC waves at frequencies of ~1 and 0.4 Hz at the low- (~63° MLAT) and high- (~64° MLAT) latitude IPA crossings at 0532–0544 UT and at 0546–0549 UT, respectively. The frequencies of these two EMIC wave signals correspond to the proton- and helium-bands, respectively. Sakaguchi et al. (2008) showed that the occurrence region of IPA tends to shift to lower (higher) latitudes

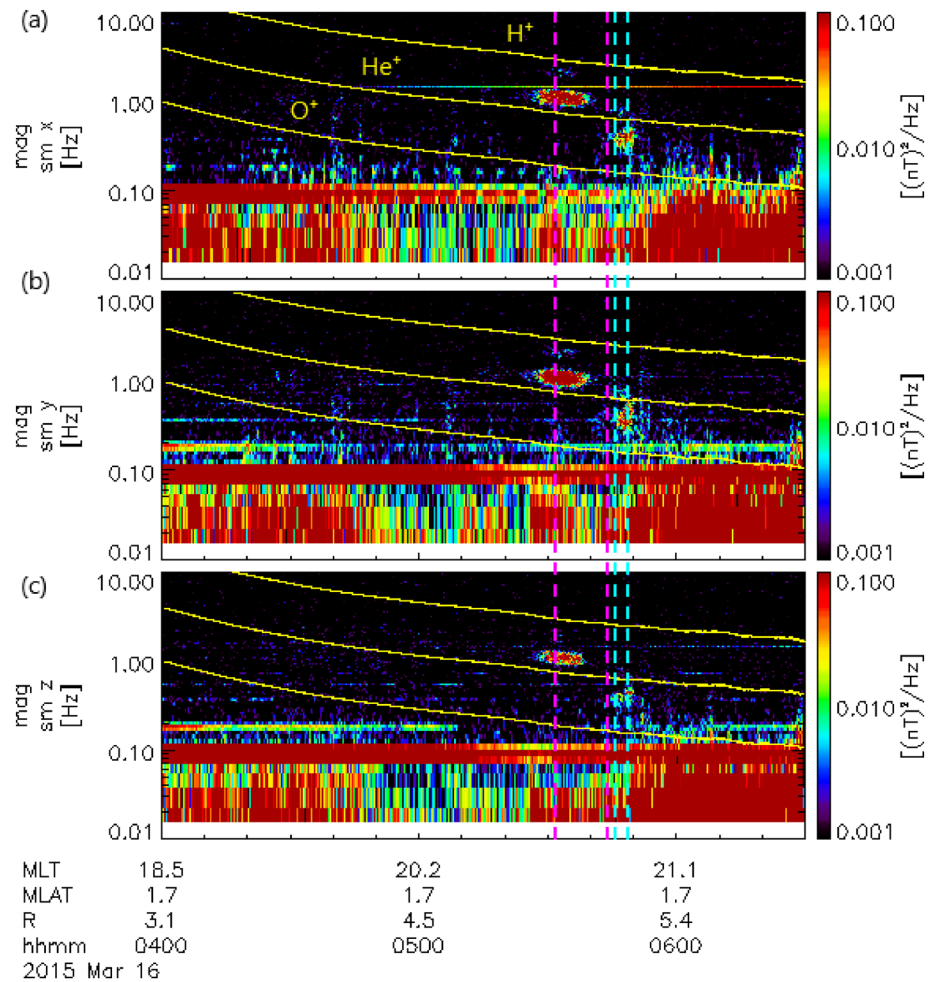


Figure 7. (a) X, (b) Y, and (c) Z components of magnetic field spectra in S M coordinates obtained at 0400–0630 UT on March 16, 2015 by Van Allen Probes (Probe A). Pink and cyan dotted lines show time intervals when the footprint of the Van Allen Probes crossed over the two IPAs. Yellow lines show the cyclotron frequencies of H⁺, He⁺, and O⁺.

with increasing (decreasing) frequency of simultaneous Pc1/EMIC waves on the ground, and the relationship between IPA latitudes and EMIC wave frequencies in this study agrees with their results. However, the induction magnetometer on the ground did not observe the Pc1/EMIC wave at a frequency of ~ 1 Hz (proton-band), while it did observe the ~ 0.4 -Hz (helium-band) wave. Perraut et al. (1984) reported that it is difficult for proton-band EMIC waves to propagate to the ground, but helium-band waves do propagate to the ground. This is consistent with the results of this study.

In this event, there is a time lag between the IPA crossings and the appearances of the EMIC waves in Figures 5c, 5d, and 7. The start of the IPA crossings at 0532 UT (shown by the pink dashed line) is ~ 4 min delayed from the EMIC wave start at 0528 UT, corresponding to the latitudinal difference of $\sim 0.1^\circ$ in the ionospheric footprint. This time delay (or spatial difference) may be due to (1) ambiguity of the field-line mapping of the satellite footprint to the ionosphere. For example, the footprint location can differ $\sim 1^\circ$ in latitudes between IGRF and T01 models. The second possibility is (2) time interval necessary for protons precipitation from the magnetosphere to the ionosphere. In this event, the time of the proton precipitation (5–20 keV) was estimated to be ~ 12 –24 s. This value is much smaller than the observed time difference (4 min). The third possibility is (3) protons motion across magnetic field lines due to $E \times B$ drift. In that case, the $E \times B$ drift velocity can be estimated to be 460–920 m/s (0.1° in latitude divided by 12–24 s precipitation time). These values seem to be higher than typical north-south convection velocities at subauroral latitudes. The other possibility is that (4) hydrogen atom is not trapped by magnetic field lines, causing the expansion

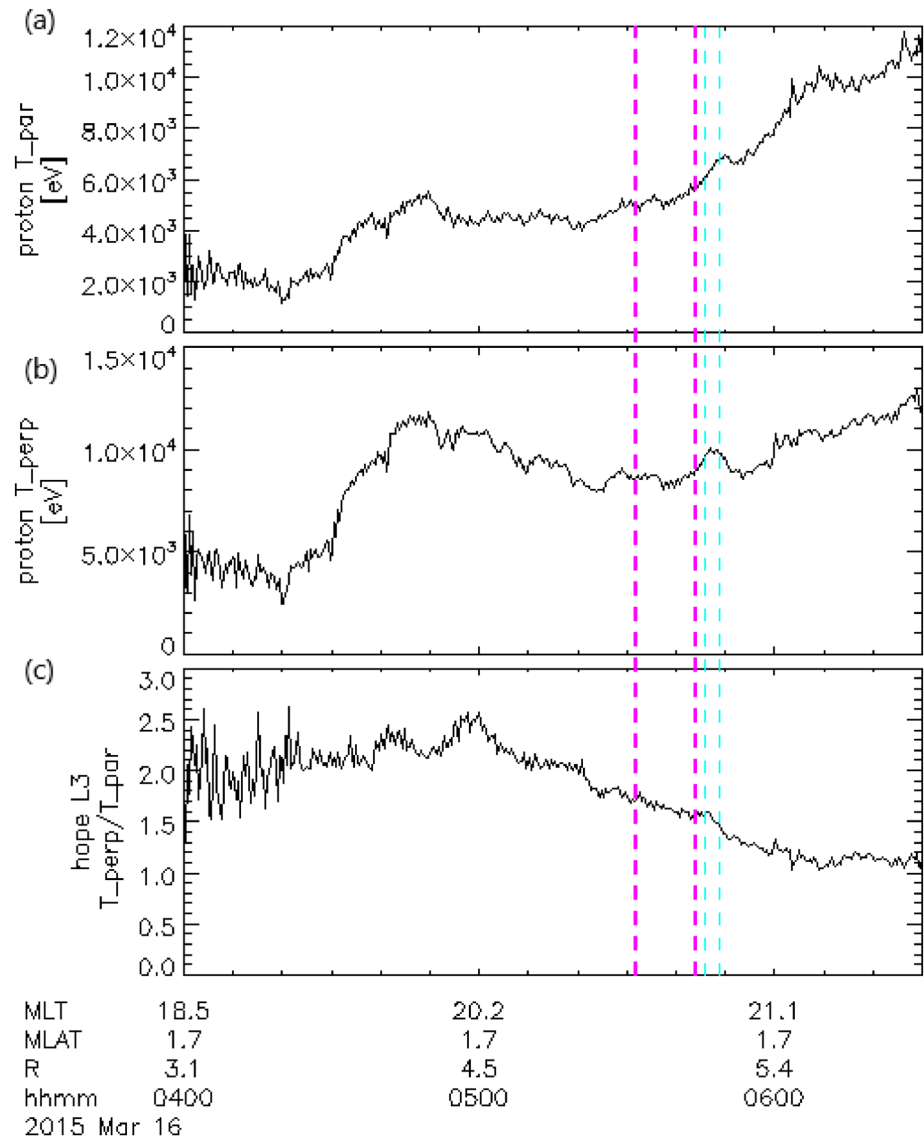


Figure 8. (a) Proton temperature parallel to the magnetic field line (T_{par}) and (b) perpendicular to the magnetic field line (T_{perp}) and (c) proton temperature anisotropy ($T_{\text{perp}} / T_{\text{par}}$) observed at 0400–0630 UT on March 16, 2015 by Van Allen Probes (Probe A). Pink and cyan dotted lines show time intervals when the Van Allen Probes footprint crossed over the two IPAs.

of the auroral emission region from the precipitation region. However, this process does not cause the observed systematic shift of the IPA location to latitudes higher than the EMIC region. From these considerations, we consider that the observed time lag/spatial difference between IPA and EMIC regions is due to ambiguity of the field-line mapping.

In Figure 5a, proton flux responsible for the ring current at energies of 5–20 keV increases rapidly during the interval of the IPA crossings. This may be due to injection of hot plasma from the magnetotail by previous substorms. Since proton flux locally increased, it is possible that injected protons in a previous substorm are concentrated at a specific L value range during their longitudinal drift. The low-energy electron flux enhancement in Figure 5b in the same L range may be also caused by the same previous substorm injection. Associated with the rapid increase of proton fluxes, the Van Allen Probes observed EMIC waves at frequencies of ~ 1 and 0.4 Hz. The proton temperature anisotropy at energies of 1 eV–50 keV was 1.5–2.5 at 0400–0500 UT, gradually decreasing from 0500 to 0600 UT. The temperature anisotropy of ions drives EMIC

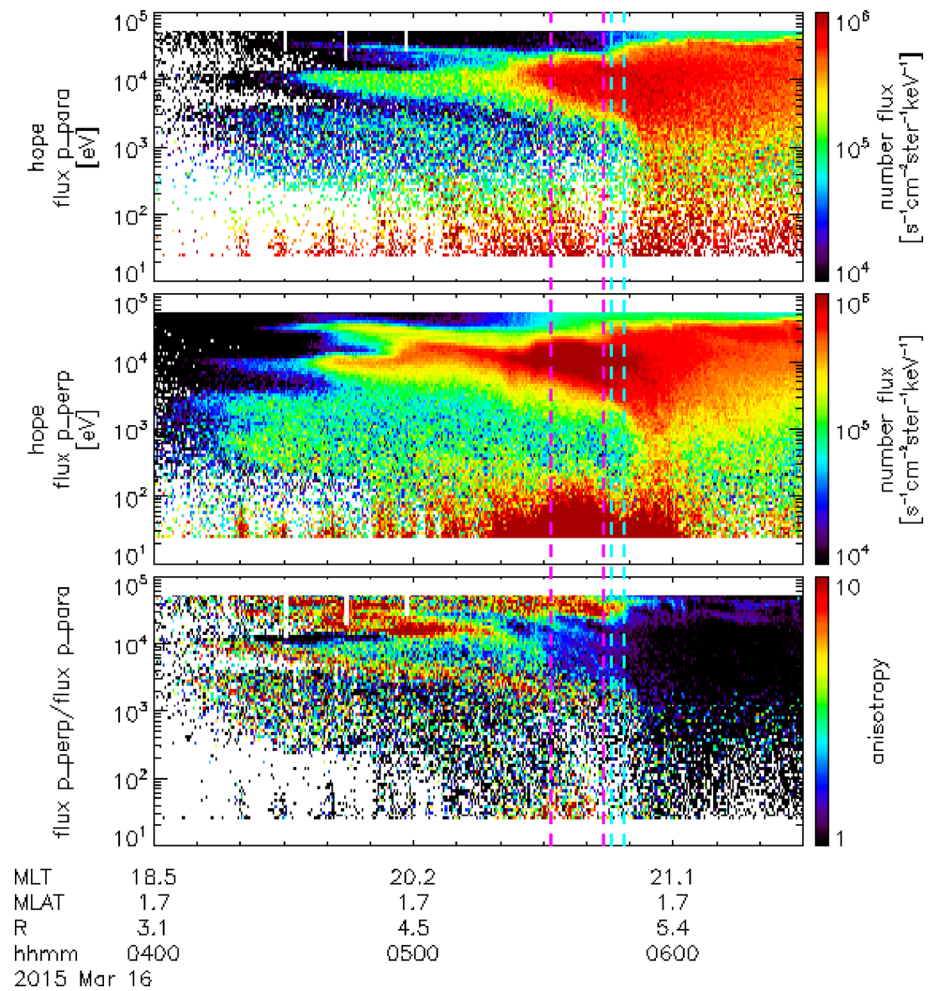


Figure 9. Proton number flux (a) parallel and (b) perpendicular to the magnetic field line and (c) ratio (anisotropy) of perpendicular flux divided by the parallel flux, observed at 0400–0630 UT on March 16, 2015 by Van Allen Probes (Probe A). Pink and cyan dotted lines show time intervals when the Van Allen Probes footprint crossed over the two IPAs.

wave growth. Namely, if anisotropy is sufficiently high, the wave will grow to scatter the pitch angle of protons to reduce anisotropy (Cornwall et al., 1970). The EMIC waves can thus grow in this region. However, Figures 8 and 9 indicate no particular enhancement of temperature anisotropy when the Van Allen Probes observed the two localized EMIC waves.

Plasmaspheric plumes or plasmopause are locations where EMIC waves strengthen. In this study, EMIC waves were observed near the plasmopause, consistent with previous studies (e.g., Fraser et al., 2009). IPAs observed on the ground extended in the longitudinal direction, so the EMIC waves likely occurred along the plasmopause. In addition, electron density at the time of the IPA crossings was in the plasmopause region just before the sharp decrease. The surrounding plasma density is known to greatly influence resonance conditions of waves and ions (e.g., Miyoshi et al., 2008). Therefore, we conclude that local increase of proton flux at a specific energy range (5–20 keV) and local structure of the electron density near the plasmopause contribute to the generation of localized IPAs in a narrow latitudinal width.

In the case of electron auroral arcs in the auroral oval, it is understood that shear of plasma flow corresponding to the converging electric field forms upward field-aligned current and associated auroral arcs (e.g., Hasegawa & Sato, 1979). Generally, large DC magnetic field variations of several hundred nanoTeslas have been observed when satellites cross auroral arcs at ionospheric altitudes (e.g., Armstrong & Zmuda, 1970). In the present event, when the satellite footprint passed two IPAs, characteristic DC variations

of the electric field were not observed. On the other hand, we observed the magnetic field variations with an amplitude of ~ 2 nT in B_y and B_z at 0532–0544 UT shown by the pink dashed lines in Figure 6. The satellite moved 0.28 Re in X direction as shown in Figure 4. The field-aligned current estimated by the magnetic field observed by the satellite was $\sim 0.258 \mu\text{A}/\text{m}^2$ ($= (2 \text{ nT}/0.28 \text{ Re}/\mu_0) \times (B_I/B_M)$), $B_I = 54,225.7$ nT, $B_M = 187.45$ nT, $\mu_0 = 1.256 \times 10^{-6} \text{ NA}^{-2}$. This indicates that the observed IPAs were accompanied by a weak field-aligned current which was one order smaller than the typical field-aligned currents in the auroral oval ($1\text{--}2 \mu\text{A}/\text{m}^2$, e.g., Iijima & Potemra, 1978).

6. Conclusions

In this study, we investigated simultaneous ground-satellite observations of IPAs associated with Pc1 geomagnetic pulsations at subauroral latitudes, using an all-sky imager at Athabasca and Van Allen Probes (Probe A) for the 6 years of 2013–2018. One simultaneous observation event was identified during the recovery phase of a substorm on March 16, 2015. No such simultaneous ground-satellite observations of IPAs and their associated plasma and electromagnetic fields in the source magnetosphere have been previously reported. The following summarizes the results of this study:

1. The Van Allen Probes footprint passed over two IPAs at 0532–0544 UT and at 0546–0549 UT. Respectively corresponding to these timings, the Van Allen Probes observed localized EMIC waves at frequencies of ~ 1 and 0.4 Hz near the plasmopause in the magnetic equatorial plane at a radial distance of ~ 5 Re.
2. Localized EMIC waves at frequencies of ~ 1 and 0.4 Hz in the magnetosphere correspond to IPAs at lower ($\sim 63^\circ$ MLAT) and higher ($\sim 64^\circ$ MLAT) latitudes. However, the wave at a frequency of ~ 1 Hz was not observed on the ground, while the EMIC wave at a frequency of ~ 0.4 Hz was observed. We consider this to be because the EMIC wave at ~ 1 Hz was a proton-band that hardly propagates to the ground.
3. Corresponding to these localized EMIC waves, the proton flux at an energy range of 5–20 keV locally increased. The ambient electron density at the time of these IPA crossings was just before the sharp decrease in the plasmopause region. The proton temperature anisotropy was 1.5–2.5 at 0400–0545 UT. However, the temperature anisotropy does not show the characteristic enhancement associated with these localized EMIC waves. We conclude that proton flux increase at a specific energy range and the plasmopause structure greatly contribute to the latitudinally localized appearance of EMIC waves and IPAs. This locally enhanced proton flux may be due to drifting particles injected by a previous substorm.
4. The Van Allen Probes did not observe converging electric fields, and observed magnetic field variations at the time scale of the IPA crossings. This result suggests that the IPAs caused by EMIC waves were accompanied by a weak field-aligned current.

Data Availability Statement

Data from the ground-based instruments at Athabasca are available at these websites. The authors thank NASA's Van Allen Probe team for the use of EFW Level 2 and 3 data products (<http://www.space.umn.edu/missions/rbsp-efw-home-university-of-minnesota/>), EMFISIS data (<https://emfis.physics.uiowa.edu/data/index>), and the HOPE instrument plasma data (<https://www.rbsp-ect.lanl.gov/science/DataDirectories.php>). The World Data Center for Geomagnetism at Kyoto University provided the AE index.

References

- Albert, J. M. (2003). Evaluation of quasi-linear diffusion coefficients for EMIC waves in a multispecies plasma. *Journal of Geophysical Research*, 108, 1249. <https://doi.org/10.1029/2002JA009792>
- Armstrong, J. C., & Zmuda, A. J. (1970). Field-aligned current at 1100 km in the auroral region measured by satellite. *Journal of Geophysical Research*, 75, 34. <https://doi.org/10.1029/ja075i034p07122>
- Cornwall, J. M., Coroniti, F. V., & Thorne, R. M. (1970). Turbulent loss of ring current protons. *Journal of Geophysical Research*, 75, 4699–4709. <https://doi.org/10.1029/ja075i025p04699>
- Ejiri, M., Hoffman, R. A., & Smith, P. H. (1980). Energetic particle penetrations into the inner magnetosphere. *Journal of Geophysical Research*, 85, 653. <https://doi.org/10.1029/ja085ia02p00653>
- Fraser, B. J., Grew, R. S., Morley, S. K., Green, J. C., Singer, H. J., Loto'aniu, T. M., & Thomsen, M. F. (2010). Storm time observations of electromagnetic ion cyclotron waves at geosynchronous orbit: GOES results. *Journal of Geophysical Research*, 115, A05208. <https://doi.org/10.1029/2009JA014516>
- Fraser, B. J., Kemp, W. J., & Webster, D. J. (1989). Ground-satellite study of a Pc 1 ion cyclotron wave event. *Journal of Geophysical Research*, 94, 855–863. <https://doi.org/10.1029/JC094iC01p0085510.1029/ja094ia09p11855>

Acknowledgments

We thank Yasuo Katoh, Yoshiyuki Hamaguchi, Yuka Yamamoto, and Takumi Adachi, technical staff of the ISEE at Nagoya University, and Ian Schofield of Athabasca University for their helpful support in operating the ground-based instruments at Athabasca, Canada. Database construction for the ground-based instruments used in the present study was supported by the ERG Science Center (<https://ergsc.isee.nagoya-u.ac.jp/>) and the Inter-university Upper atmosphere Global Observation Network project (<http://www.iugonet.org/>). The observatory at Athabasca was constructed with, and is operated with the support of, the Canada Foundation for Innovation. This work is supported by JSPS KAKENHI (15H05815, 16H06286, 20H01959).

- Funsten, H. O., Skoug, R. M., Guthrie, A. A., MacDonald, E. A., Baldonado, J. R., Harper, R. W., et al. (2013). Helium, oxygen, proton, and electron (HOPE) mass spectrometer for the Radiation Belt Storm Probes Mission. *Space Science Reviews*, 179, 423–484. <https://doi.org/10.1007/s11214-013-9968-7>
- Hasegawa, A., & Sato, T. (1979). Generation of field aligned current during substorm. *Dynamics of the Magnetosphere*, 529–542. https://doi.org/10.1007/978-94-009-9519-2_28
- Horne, R. B., & Thorne, R. M. (1993). On the preferred source location for the convective amplification of ion cyclotron waves. *Journal of Geophysical Research*, 98, 9233–9247. <https://doi.org/10.1029/92JA02972>
- Iijima, T., & Potemra, T. A. (1978). Large-scale characteristics of field-aligned currents associated with substorms. *Journal of Geophysical Research*, 83, 7A0898. <https://doi.org/10.1029/ja083ia02p00599>
- Keika, K., Takahashi, K., Ukhorskiy, A. Y., & Miyoshi, Y. (2013). Global characteristics of electromagnetic ion cyclotron waves: Occurrence rate and its storm dependence. *Journal of Geophysical Research: Space Physics*, 118, 4135–4150. <https://doi.org/10.1002/jgra.50385>
- Kletzing, C. A., Kurth, W. S., Acuna, M., MacDowall, R. J., Torbert, R. B., Averkamp, T., et al. (2013). The electric and magnetic field instrument suite and integrated science (EMFISIS) on RBSP. *Space Science Reviews*, 179, 127–181. <https://doi.org/10.1007/s11214-013-9993-6>
- Min, K., Lee, J., Keika, K., & Li, W. (2012). Global distribution of EMIC waves derived from THEMIS observations. *Journal of Geophysical Research*, 117, A05219. <https://doi.org/10.1029/2012JA017515>
- Miyoshi, Y., Matsuda, S., Kurita, S., Nomura, K., Keika, K., Shoji, M., et al. (2019). EMIC waves converted from equatorial noise due to $M/Q = 2$ ions in the plasmasphere: Observations from Van Allen Probes and Arase. *Geophysical Research Letters*, 46, 5662–5669. <https://doi.org/10.1029/2019GL083024>
- Miyoshi, Y., Sakaguchi, K., Shiokawa, K., Evans, D., Albert, J., Connors, M., & Jordanova, V. (2008). Precipitation of radiation belt electrons by EMIC waves, observed from ground and space. *Geophysical Research Letters*, 35, L23101. <https://doi.org/10.1029/2008GL035727>
- Morley, S. K., Ables, S. T., Sciffer, M. D., & Fraser, B. J. (2009). Multipoint observations of Pc1-2 waves in the afternoon sector. *Journal of Geophysical Research*, 114, A09205. <https://doi.org/10.1029/2009JA014162>
- Nishimura, Y., Bortnik, J., Li, W., Lyons, L. R., Donovan, E. F., Angelopoulos, V., & Mende, S. B. (2014). Evolution of nightside subauroral proton aurora caused by transient plasma sheet flows. *Journal of Geophysical Research: Space Physics*, 119, 5295–5304. <https://doi.org/10.1002/2014JA020029>
- Nomura, R., Shiokawa, K., Sakaguchi, K., Otsuka, Y., & Connors, M. (2012). Polarization of Pc1/EMIC waves and related proton auroras observed at subauroral latitudes. *Journal of Geophysical Research*, 117. <https://doi.org/10.1029/2011JA017241>
- Omura, Y., & Zhao, Q. (2012). Nonlinear pitch angle scattering of relativistic electrons by EMIC waves in the inner magnetosphere. *Journal of Geophysical Research*, 117, A08227. <https://doi.org/10.1029/2012JA017943>
- Omura, Y., & Zhao, Q. (2013). Relativistic electron microbursts due to nonlinear pitch angle scattering by EMIC triggered emissions. *Journal of Geophysical Research: Space Physics*, 118, 5008–5020. <https://doi.org/10.1002/jgra.50477>
- Perraut, S., Gendrin, R., Roux, A., & de Villedary, C. (1984). Ion cyclotron waves: Direct comparison between ground-based measurements and observations in the source region. *Journal of Geophysical Research*, 89, 195–202. <https://doi.org/10.1029/ja089ia01p00195>
- Pickett, J. S., Grison, B., Omura, Y., Engebretson, M. J., Dandouras, I., Masson, A., et al. (2010). Cluster observations of EMIC triggered emissions in association with Pc1 waves near Earth's plasmapause. *Geophysical Research Letters*, 37, L09104. <https://doi.org/10.1029/2010GL042648>
- Sakaguchi, K., Shiokawa, K., Ieda, A., Miyoshi, Y., Otsuka, Y., Ogawa, T., et al. (2007). Simultaneous ground and satellite observations of an isolated proton arc at subauroral latitudes. *Journal of Geophysical Research*, 112(A04202). <https://doi.org/10.1029/2006JA012135>
- Sakaguchi, K., Shiokawa, K., Miyoshi, Y., Otsuka, Y., Ogawa, T., Asamura, K., & Connors, M. (2008). Simultaneous appearance of isolated auroral arcs and Pc 1 geomagnetic pulsations at subauroral latitudes. *Journal of Geophysical Research*, 113, A05201. <https://doi.org/10.1029/2007JA012888>
- Sakaguchi, K., Shiokawa, K., Miyoshi, Y., & Connors, M. (2016). Isolated proton auroras and Pc1/EMIC waves at subauroral latitudes, auroral dynamics and space weather. *Geophysical Monograph*, 215, 59–70.
- Shepherd, S. G. (2014). Altitude-adjusted corrected geomagnetic coordinates: Definition and functional approximations. *Journal of Geophysical Research: Space Physics*, 119, 7501–7521. <https://doi.org/10.1002/2014JA020264>
- Shiokawa, K., Katoh, Y., Satoh, M., Ejiri, M. K., Ogawa, T., Nakamura, T., et al. (1999). Development of optical mesosphere thermosphere imagers (OMTI). *Earth, Planets and Space*, 51, 887–896. <https://doi.org/10.1186/bf03353247>
- Shiokawa, K., Nomura, R., Sakaguchi, K., Otsuka, Y., Hamaguchi, Y., Satoh, M., et al. (2010). The STEL induction magnetometer network for observation of high-frequency geomagnetic pulsations. *Earth, Planets and Space*, 62, 517–524. <https://doi.org/10.5047/eps.2010.05.003>
- Smith, P. H., & Hoffman, R. A. (1974). Direct observations in the dusk hours of the characteristics of the storm time ring current particles during the beginning of magnetic storms. *Journal of Geophysical Research*, 79, 966–971. <https://doi.org/10.1029/ja079i007p00966>
- Spence, H. E., Reeves, G. D., Baker, D. N., Blake, J. B., Bolton, M., Bourdarie, S., et al. (2013). Science goals and overview of the Radiation Belt Storm Probes (RBSP) Energetic Particle, Composition, and Thermal Plasma (ECT) Suite on NASA's Van Allen Probes Mission. *Space Science Reviews*, 179, 311–336. <https://doi.org/10.1007/s11214-013-0007-5>
- Summers, D., & Thorne, R. M. (2003). Relativistic electron pitch-angle scattering by electromagnetic ion cyclotron waves during geomagnetic storms. *Journal of Geophysical Research*, 108(1143). <https://doi.org/10.1029/2002JA009489>
- Thébault, E., Finlay, C. C., Beggan, C. D., Alken, P., Aubert, J., Barrois, O., et al. (2015). International geomagnetic reference field: The 12th generation. *Earth, Planets and Space*, 67, 79. <https://doi.org/10.1186/s40623-015-0228-9>
- Thorne, R. M., Horne, R. M., Jordanova, V. K., Bortnik, J., & Glauert, S. (2006). Interaction of EMIC waves with thermal plasma and radiation belt particles. *Geophysical Monograph Series*, 169. <https://doi.org/10.1029/169GM14>
- Tsyganenko, N. A. (2002a). A model of the near magnetosphere with a dawn-dusk asymmetry 1. Mathematical structure. *Journal of Geophysical Research*, 107, SMP 12-1–SMP 12-15. <https://doi.org/10.1029/2001JA000219>
- Tsyganenko, N. A. (2002b). A model of the near magnetosphere with a dawn-dusk asymmetry 2. Parameterization and fitting to observations. *Journal of Geophysical Research*, 107, SMP 10-1–SMP 10-17. <https://doi.org/10.1029/2001JA000220>
- Tsyganenko, N. A., & Sitnov, M. I. (2005). Modeling the dynamics of the inner magnetosphere during strong geomagnetic storms. *Journal of Geophysical Research*, 110, A03208. <https://doi.org/10.1029/2004JA010798>
- Usanova, M. E., Darrouzet, F., Mann, I. R., & Bortnik, J. (2013). Statistical analysis of EMIC waves in plasmaspheric plumes from cluster observations. *Journal of Geophysical Research: Space Physics*, 118, 4946–4951. <https://doi.org/10.1002/jgra.50464>
- Vegard, L. (1939). Hydrogen showers in the auroral region. *Nature*, 144, 1089.
- Wygant, J. R., Bonnell, J. W., Goetz, K., Ergun, R. E., Mozer, F. S., Bale, S. D., et al. (2013). The electric field and waves instruments on the Radiation Belt Storm Probes mission. *Space Science Reviews*, 179, 183–220. <https://doi.org/10.1007/s11214-013-0013-7>

- Yahnin, A. G., Yahnina, T. A., & Frey, H. U. (2007). Subauroral proton spots visualize the Pc1 source. *Journal of Geophysical Research*, *112*, A10223. <https://doi.org/10.1029/2007JA012501>
- Yahnina, T. A., Yahnin, A. G., Kangas, J., & Manninen, J. (2000). Proton precipitation related to Pc1 pulsations. *Geophysical Research Letters*, *27*, 3575–3578. <https://doi.org/10.1029/2000gl003763>
- Yahnina, T. A., Yahnin, A. G., Kangas, J., & Manninen, J. (2002). Localized enhancements of energetic proton fluxes at low altitudes in the subauroral region and their relation to the Pc1 pulsations. *Cosmic Research*, *40*, 213–223. <https://doi.org/10.1023/a:1015968702640>
- Yahnina, T. A., Yahnin, A. G., Kangas, J., Manninen, J., Evans, D. S., Demekhov, A. G., et al. (2003). Energetic particle counterparts for geomagnetic pulsations of Pc1 and IPDP types. *Annals of Geophysics*, *21*, 2281–2292. <https://doi.org/10.5194/angeo-21-2281-2003>